JETP Letters, Vol. 75, No. 6, 2002, pp. 268–272. Translated from Pis'ma v Zhurnal Éksperimental'noĭ i Teoreticheskoĭ Fiziki, Vol. 75, No. 6, 2002, pp. 318–322.


# Observing Remanent States of Small Magnetic Particles: Micromagnetic Simulation and Experiment

**A. M. Alekseev[1], V. A. Bykov[1], A. F. Popkov[1,*], N. I. Polushkin[2], and V. I. Korneev[3]**

[1]*State Research Center of Russian Federation–State Research Institute for Problems in Physics, NT MDT, Moscow, 103460 Russia*

[2]*Institute of Microstructure Physics, Russian Academy of Science, Nizhnii Novgorod, 603950 Russia*

[3]*Moscow Institute of Electronic Engineering (Technological University), Moscow, 103482 Russia*

**e-mail: popkov@nonlin.msk.ru*

**Abstract**—Micromagnetic properties of submicron ferromagnetic elements ellipsoidal in shape are studied theoretically and experimentally. By numerically solving the equations of magnetodynamics, it is found that different remanent magnetization states can be obtained, depending on the way of magnetization reversal in such elements: one-vortex states, two-vortex states, and vortex-free states with skew-symmetric spin pinning. The magnetization configurations predicted in the calculations have been observed experimentally using magnetic force microscopy in regular lattices of microstructures formed in thin-film samples of Fe–Cr alloys under irradiation by interfering laser beams. © *2002 MAIK "Nauka/Interperiodica".*

PACS numbers: 67.80.Jd, 75.60.Ej

**1.** It is known that nonuniform vortex magnetization configurations arise in small (ferro)magnetic particles with low magnetic crystalline anisotropy and sizes exceeding the absolute single-domain threshold (~0.05 μm) [1, 2]. The distribution of magnetic moments observed in the remanent state depends essentially on the magnetization prehistory and on the particle shape and size. Recently, new, primarily lithographic technologies have evolved for obtaining thin-film elements with planar sizes down to several tens of nanometers and their regular lattices with a given geometry [3, 4]. Progress in the field of nanotechnologies has stimulated studies of micromagnetism in small particles exemplified with thin-film magnetic elements (see, for example, [5–8]). These works are devoted to both the occurrence of vortex configurations primarily in elements rectangular in shape and the states of new type, so-called *C* and *S* configurations, that are characterized by boundary spin pinning due to the magnetostatic effect of element boundaries. The boundary pinning effect is manifested in the multimode character of magnetization reversal, which can be the reason for the giant instability of switching fields associated with the thermally activated change of the magnetization reversal mode in the vicinity of the saturation state [8]. The use of elements of nonrectangular, in particular, ellipsoidal shape, in which the formation of alternative magnetization configurations associated with spin pinning in the vicinity of narrow poles of the magnetized element is not highly probable, is one of the ways for suppressing this instability. It is these elements that are formed, for example, under irradiation of a finely dispersed superparamagnetic Fe–Cr medium by interfering laser beams [9]. A regular lattice of ferromagnetic elements is formed at interference maxima as a result of modification of magnetic properties. The technology of obtaining such a structured medium was described previously in [9]. The goal of this work was (1) to simulate possible remanent magnetization states in submicron elements of ellipsoidal shape and (2) to compare the results of simulation with experimental data for magnetic lattices obtained in studying thin-film Fe–Cr alloys using a magnetic force microscope (MFM).

**2. Magnetization of ellipsoidal particles.** The magnetization reversal processes in flat microparticles were analyzed theoretically by numerically integrating the Landau–Lifshitz equations with free boundary conditions. The scheme of numerical integration and examples of modeling rectangular particles were described previously in our works [7, 8, 10]. It was possible to vary the element sizes and the magnetic anisotropy parameters in the calculations. In this work, we will report the results of modeling an elliptic flat element $0.6 \times 0.3 \times 0.015$ μm in size with zero magnetic anisotropy. The magnetic parameters adopted in the calculation, namely, the saturation magnetization $M = 1300$ G and the nonuniform exchange constant $A = 10^{-6}$ erg/cm$^3$ corresponded to experimental data for Fe–Cr films.

Modeling the process of magnetization along the long element axis (easy direction of magnetization) showed that the main magnetic hysteresis loop has a rectangular shape for a particle of a specified size and that a uniformly magnetized particle is switched in the field $H_{c1} = 300$ Oe. The magnitude of this field grows as the film thickness and the element aspect ratio increase. The remanent state corresponds to the complete mag-

0021-3640/02/7506-0268$22.00 © 2002 MAIK "Nauka/Interperiodica"

netic polarization of the particle in the easy direction (Fig. 1a).

Magnetization in the transverse direction is of a more complicated character. In this work, we studied the variation of the state of initial magnetization along the long element axis shown in Fig. 1a upon applying a magnetic field along the short axis (hard direction of magnetization). As the magnetic field increases, a smooth rotation of spins occurs at the center of the particle and a skew-symmetric state with spins pinned at the element boundaries (Fig. 1b). The region of nonuniform magnetization variation in the vicinity of pinned regions is narrowed down as the field increases. The calculations demonstrate that the curve of transverse magnetization is of a reversible character up to the critical field $H_{c2} = 950$ Oe and that the initially polarized state is restored as the magnetic field goes to zero. When the critical field $H_{c2}$ is exceeded, the particle transforms into a state saturated in the transverse direction and the initial polarization is not restored. The effect of spin pinning at the element boundaries leads to a delay in the transition to the saturated state as compared to the uniform spin rotation model by Stoner and Wohlfarth [11], which takes into account the effect of only film demagnetizing factors. The critical depinning field $H_{c2}$ grows with increasing film thickness stronger than the critical magnetization reversal field in the transverse direction $H_{c1}$. The latter depends very strongly on the aspect ratio and sharply increases with decreasing element width.

As the magnetic field decreases from the saturation state of a transversely magnetized particle, a tendency is observed toward a turn of the magnetization at the center of the element, and, as the field goes to zero, a remanent skew-symmetric state is formed that is characterized by partial magnetic depolarization of the particle along the easy direction (Fig. 1c). As the sign of the magnetic field changes, this state is stable up to the critical field $H_{c3} = 50$ Oe, above which a transition to a two-vortex state takes place. The center of the particle undergoes backward magnetization reversal, and the effect of boundary magnetostatic spin pinning leads to the formation of two oppositely wound magnetic vortices in the vicinity of element points. When the field returns to zero, this state transforms into a demagnetized remanent state characterized by two magnetic vortices located at the corners of a diamond-shaped domain at the center of the element with magnetization directed across the element (Fig. 1d). If an element resides in a remanent two-vortex state, then, as the magnetic field increases in the transverse direction, the vortices are gradually expelled from the element and it transforms into a state saturated in the transverse direction at fields exceeding the critical saturation field in the transverse direction $H_{c4} = 1650$ Oe. Before the transition into a state saturated in the transverse direction (in fields $H < H_{c4}$), given field noise fluctuations or field nonuniformity, the element transforms into a close-in-

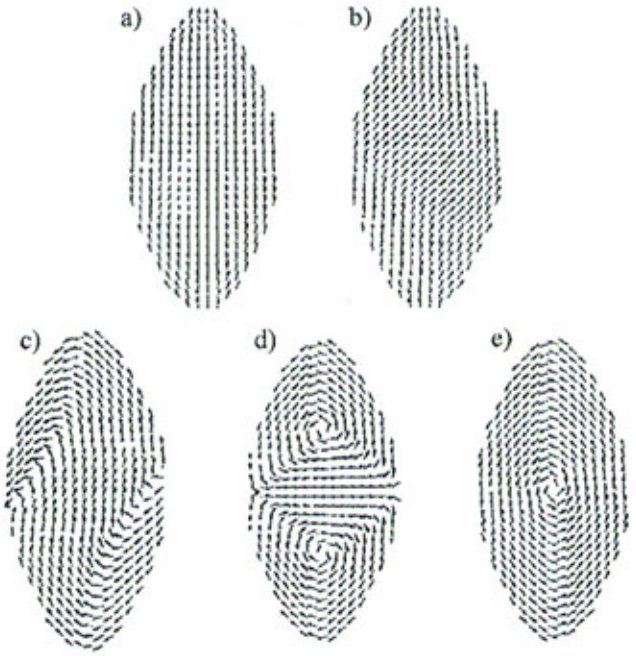


**Fig. 1.** Calculated magnetic configurations of a Fe–Cr ellipsoidal particle ($0.6 \times 0.3 \times 0.15$ μm) arising in the process of its magnetization in the traverse direction: (a) initial remanent state magnetically polarized along the easy direction, (b) spin pinning state under weak magnetization in the traverse direction for $H < H_{c2}$, (c) remanent state with skew-symmetric spin pinning, (d) two-vortex remanent state, and (e) one-vortex remanent state.

energy, more stable, asymmetric one-vortex state, which transforms into a symmetric demagnetized state with a vortex at the center of the element as the field returns to zero (Fig. 1e). Some of the states described above and shown in Fig. 1 were observed experimentally in MFM images.

**3. Observing remanent states using MFM.** In order to compare the model distributions with the results of visualizing images using an MFM, we calculated these images corresponding to micromagnetic configurations. The simulation was carried out under the assumption that the interaction of the magnetically rigid point tip of the force microscope needle with the distributed magnetic subsystem of the flat ultrathin element is of the magnetic dipole character. A point magnetic dipole located at height $x$ above the plane of the element creates a magnetic field in its plane

$$\mathbf{H} = \frac{V}{4\pi}\left(\frac{\mathbf{M}_1}{r^3} - \frac{3(\mathbf{M}_1 \cdot \mathbf{r})\mathbf{r}}{r^5}\right), \quad (1)$$

where $\mathbf{M}_1$ is the magnetization of the MFM needle, $V$ is the volume of the magnetic tip, $r = [(x - x')^2 + (y - y')^2 + z^2]^{1/2}$ is the distance from the tip (above the sighting point (x, y)) to an arbitrary point $(x', y')$ in the plane of the sample $z = 0$. The Zeeman energy of interaction with a thin magnetic layer of thickness $t$ having the

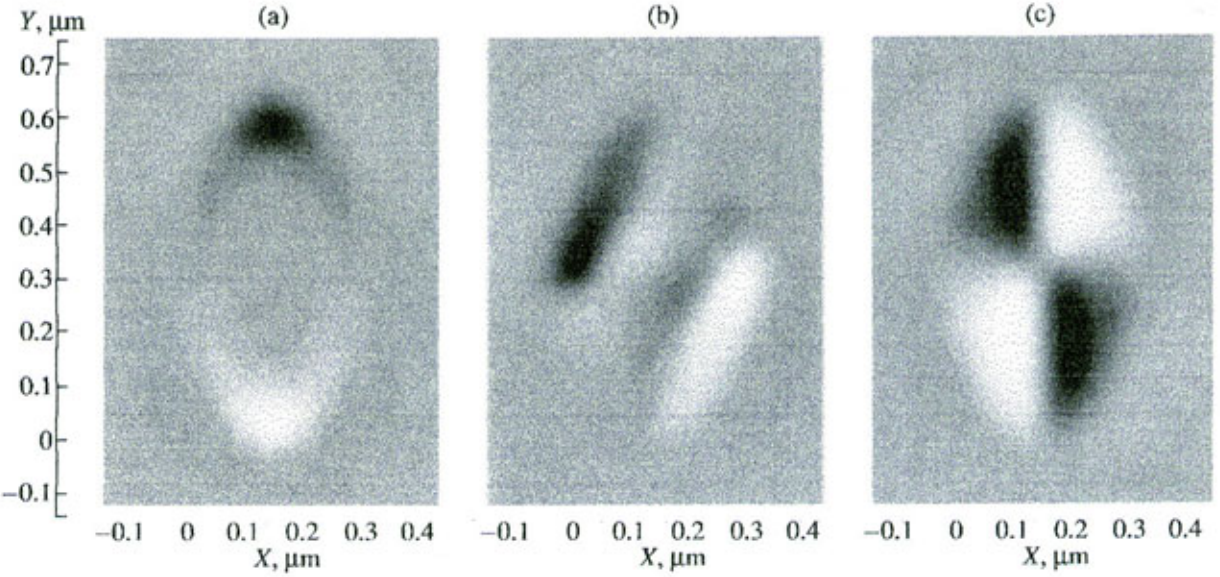


**Fig. 2.** Calculated MFM images of remanent configurations shown in Fig. 1: (a) magnetically polarized particle, (b) skew-symmetric state with boundary spin pinning, an (c) one-vortex demagnetized state.

magnetic configuration $\mathbf{M}_2(x', y')$ is given by the convolution $E(x, y) = t\mu_0 \int \mathbf{M}_2(x', y') \cdot \mathbf{H}(x - x'. y - y')dx'dy'$, where integration is carried out over the plane of the sample. The signal of an MFM using resonance oscillations of a cantilever is proportional to the second variation of the Zeeman energy of interaction of the magnetic needle with the field of the sample [12]. Therefore, one can write

$$\Delta\Omega \sim \partial_z^2 E(x, y, z)$$
$$= t\mu_0 \int_S \mathbf{M}_2(x', y') \cdot \partial_z^2 \mathbf{H}(x - x', y - t')dx'dy', \quad (2)$$

where $S$ is the area of integration.

MFM images obtained in this way at $z = 0.1$ μm are given in Fig. 2 for (a) a uniformly polarized element, (b) a vortex-free state with skew-symmetric spin pinning, and (c) a one-vortex state that correspond to the magnetization configurations depicted in Figs. 1a, 1c, and 1e.

Experimental MFM measurements were performed using a Solver P47 scanning probe microscope (NT MDT, Moscow). Topographies obtained experimentally for ferromagnetic structures formed in a (super)paramagnetic Fe–Cr layer by interfering laser beams and the corresponding MFM images are shown in Fig. 3. Topographic images (a, c, e) demonstrate surface modifications of an elliptic shape. These modifications correspond to pronounced MFM contrast (b, d, f). A uniformly polarized remanent state obtained by saturating an element along the easy axis in a field of 500 Oe is shown in Fig. 3b. A vortex-free state with skew-symmetric spin pinning was obtained experimentally by magnetization reversal of elements along their short axis in a field of 1000 Oe (Fig. 3d). It is also interesting to mention the possibility of obtaining a one-vortex remanent state (Fig. 3f) upon magnetization reversal in the transverse direction in a field of 750 Oe. Thus, the experimental data are in good agreement with the results of micromagnetic modeling.

**4.** Thus, micromagnetic modeling showed that a particle magnetized along the easy axis, being undergone transverse magnetization, retains the remanent state determined by the effect of skew-symmetric boundary spin pinning up to the critical field above which the irreversible transition to the saturation state takes place. This field essentially exceeds the switching field in the longitudinal direction. Both critical fields decrease with decreasing film thickness.

After saturation in the transverse direction, the particle does not return to the complete polarization state. In this case, two types of remanent states are possible. One of them is characterized by a spin distribution with skew-symmetric pinning at the element boundaries, and the other one corresponds to the complete demagnetization of the particle and contains either two magnetic vortices at the boundaries of the diamond-shaped magnetostatic domain inside the particle or one vortex at its center. This last-mentioned effect is in agreement with the calculations reported in [1] for a flat rectangular Permalloy particle with a large aspect ratio. It was shown in [1] that a long rectangular particle after saturation in the transverse direction is subdivided into a number of oppositely wound magnetic vortices. The application of a magnetic field leads to a gradual displacement of vortices to the element boundaries and to their disappearance at the transition to the saturated state. The effect of restoring the initial state depends on

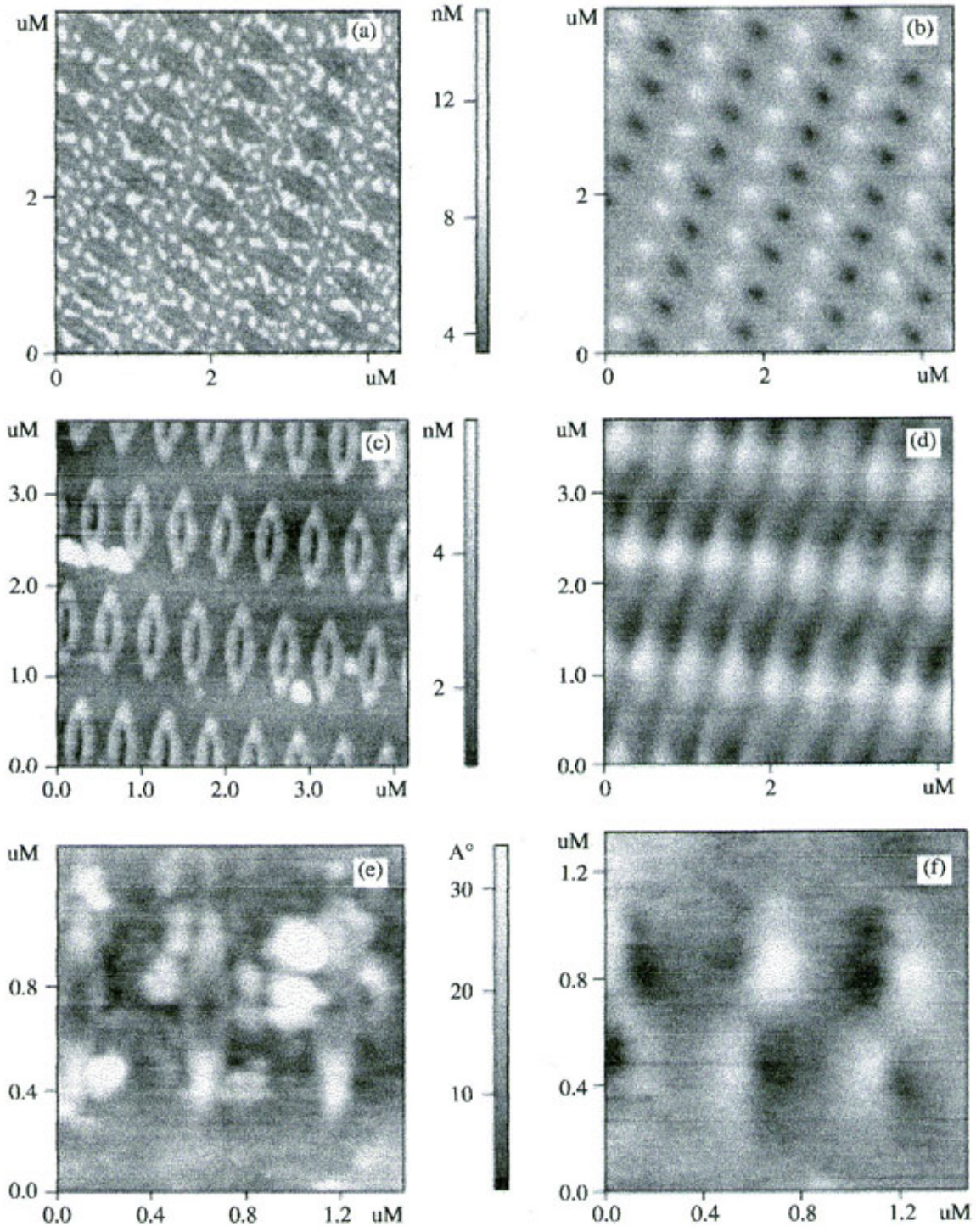


**Fig. 3.** Atomic force–magnetic force images of modified regions of Fe–Cr films obtained by interference laser sintering: (a), (c), and (e) topography of regions annealed at the irradiation intensity $J = 0.3$ W/cm$^2$; (b), (d), and (f) corresponding images of particles. The height of image pickup in the resonance mode $z = 0.05$ μm.

the direction of the magnetization field. As the particle sizes decrease, the effect of boundary spin pinning will be suppressed by exchange interaction and the behavior of the particle will approach the single-domain behavior. The character of magnetization reversal in this case will approach that predicted by the Stoner–Wohlfarth model.

The main features of magnetization reversal obtained by micromagnetic simulation are in agreement with the results of MFM observations. Thus, sta-

bility was observed with respect to the action of the transverse magnetic field of smaller particles, and completely demagnetized particles appeared upon reverse transverse magnetization after threshold saturation in the transverse direction. However, the theoretical model ignored the particular features of samples taken for experimental investigations of magnetization reversal processes and remanent states, namely, the effect of the superparamagnetic phase in the film surrounding ferromagnetic particles and the formation of crystalline microinclusions at high intensity of laser annealing. The superparamagnetic medium can serve as a magnetic conductor for the magnetic flux created by polarized magnetic particles, which may lead to an additional magnetostatic interaction of particles changing their switching fields. Taking into account the last-mentioned mechanism of the nanoparticle lattice effect on magnetization calls for further investigation.

This work was supported by the Russian Foundation for Basic Research, project nos. 02-02-16704 and 01-02-16445; International Science and Technology Center, project no. 1522; and INTAS, project no. 99-01839.

## REFERENCES

1. D. R. Fredkin, T. R. Koehler, J. F. Smyth, and S. Schultz, J. Appl. Phys. **69**, 5276 (1991).
2. R. Hertel and H. Kronmuller, Phys. Rev. B **60**, 7366 (1999).
3. S. Y. Chou, Proc. IEEE **85**, 652 (1997).
4. T. A. Savas, M. Farhoud, and H. I. Smith, J. Appl. Phys. **85**, 6160 (1999).
5. J.-G. Zhu and H. N. Bertram, IEEE Trans. Magn. **27**, 3553 (1991).
6. J.-L. Berchier, K. Solt, and T. Zajk, J. Appl. Phys. **55**, 487 (1984).
7. A. F. Popkov, L. L. Savchenko, N. V. Vorotnikova, *et al.*, Appl. Phys. Lett. **77**, 277 (2000).
8. A. F. Popkov, L. L. Savchenko, and N. V. Vorotnikova, Pis'ma Zh. Éksp. Teor. Fiz. **69**, 555 (1999) [JETP Lett. **69**, 596 (1999)].
9. A. M. Alekseev, Yu. K. Verevkin, N. V. Vostokov, *et al.*, Pis'ma Zh. Éksp. Teor. Fiz. **73**, 214 (2001) [JETP Lett. **73**, 192 (2001)].
10. A. F. Popkov, N. V. Vorotnikova, and A. Yu. Polozov, Mat. Model. **11**, 54 (1999).
11. E. C. Stoner and E. P. Wohlfarth, Philos. Trans. R. Soc. London, Ser. A **240**, 599 (1948).
12. P. Guethner, H. Mamin, and D. Rugar, in *Scanning Tunneling Microscopy II*, Ed. by R. Wiesendander and H.-J. Gunherodt (Springer-Verlag, Berlin, 1992), p. 151.

*Translated by A. Bagatur'yants*

SPELL: uM, nM, nanotechnologies, depinning, microinclusions